Elsevier Editorial System(tm) for Journal of Applied Geophysics
Manuscript Draft

Manuscript Number:

Title: INSIGHTS IN THE EJECTION PROCESS OF THE LOCKNE MARINE-TARGET IMPACT CRATER FROM ROCK MAGNETIC PROPERTIES IN THE LOCKNE-9 DRILL CORE THROUGH THE EJECTA FLAP

Article Type: Regular

Keywords: impact crater; rock magnetism; marine-target; flap formation process; Lockne crater

Corresponding Author: Ms. Irene Melero-Asensio,

Corresponding Author's Institution: CAB

First Author: Irene Melero-Asensio

Order of Authors: Irene Melero-Asensio; Fatima Martin-Hernandez; Jens Ormö

Abstract: The well-documented, well-preserved, and well-exposed Lockne crater is a reference crater for marine-target impact on Earth. To date, it has been subjected to 11 short core drillings and over 5000 outcrop descriptions, as well as several geophysical surveys. The rich data allows detailed analysis of the cratering and modification processes. A unique feature with Lockne is its pristine ejecta layer. The ejecta differs, however, from the typical text book example of a land target crater in that it, to great extent, is made up of relatively extensive, coherent ejecta flaps resting on a target surface with no structural rim uplift. However, little is known about the marine impact excavation process generating the flaps. Here, we provide a lithological description coupled with an analysis of the rock magnetic properties of the Lockne-9 core through the western, downrange ejecta flap. The 31.04m long drillcore shows ~23m of monomict (mafic) breccia overlying a ~5m thick mixed zone of breccia with fracture fill and matrix derived from Palaeozoic sedimentary target sequence (i.e. Lower Cambrian alum shale and conglomerate). The whole breccia package rests with sharp contact on the fractured, granitic basement. The conspicuous lithological and petrophysical differences between the overlying breccias and the basement suggest the former was transported as ejecta. The rock magnetic properties of the ejecta show a magnetic signal that must have existed before the impact event took place. Thus, during the cratering process the ejecta at the studied location was relocated en masse from the central part of the crater to form an ejecta flap, in contrast to the standard ballistic emplacement of individual particles in an ejecta curtain.

Highlights:

- Rock-magnetism reveals a high magnetisation zone of pre-impact nature
- Petrophysical characterization and description of the Lockne-9 core (central Sweden)
- Magnetic signal is dominated by magnetite/titanomagnetite
- Comparisons of affected and non-affected samples suggest a quick flap formation

INSIGHTS IN THE EJECTION PROCESS OF THE LOCKNE MARINE-TARGET IMPACT CRATER FROM ROCK MAGNETIC PROPERTIES IN THE LOCKNE-9 DRILL CORE THROUGH THE EJECTA FLAP.

IRENE MELERO-ASENSIO[1], FÁTIMA MARTÍN-HERNÁNDEZ[2,3], JENS ORMÖ[1]

[1] Centro de Astrobiología (INTA-CSIC). Carretera de Ajalvir km 4, Torrejón de Ardoz, 28850, Madrid, Spain.

[2] Dep. Geophysics, Fac. Physics, 28040 Madrid Universidad Complutense de Madrid, Spain.

[3] Instituto de Geociencias (UCM, CSIC), Fac. Physics, 28040 Madrid Spain.

Abstract: The well-documented, well-preserved, and well-exposed Lockne crater is a reference crater for marine-target impact on Earth. To date, it has been subjected to 11 short core drillings and over 5000 outcrop descriptions, as well as several geophysical surveys. The rich data allows detailed analysis of the cratering and modification processes. A unique feature with Lockne is its pristine ejecta layer. The ejecta differs, however, from the typical text book example of a land target crater in that it, to great extent, is made up of relatively extensive, coherent ejecta flaps resting on a target surface with no structural rim uplift. However, little is known about the marine impact excavation process generating the flaps. Here, we provide a lithological description coupled with an analysis of the rock magnetic properties of the Lockne-9 core through the western, downrange ejecta flap. The 31.04m long drillcore shows ~23m of monomict (mafic) breccia overlying a ~5m thick mixed zone of breccia with fracture fill and matrix derived from Palaeozoic sedimentary target sequence (i.e. Lower Cambrian alum shale and conglomerate). The whole breccia package rests with sharp contact on the fractured, granitic basement. The conspicuous lithological and petrophysical differences between the overlying breccias and the basement suggest the former was transported as ejecta. The rock magnetic properties of the ejecta show a magnetic signal that must have existed before the impact event took place. Thus, during the cratering process the ejecta at the studied location was relocated *en masse* from the central part of the crater to form an ejecta flap, in contrast to the standard ballistic emplacement of individual particles in an ejecta curtain.

***Keywords*:** impact crater; rock magnetism; marine-target; flap formation process; Lockne crater

1. Introduction

The Lockne crater is a 458Ma old (Ormö et al., 2010a) marine-target impact structure located in central Sweden (63º00'20''N, 14º49'30''E) (Figure 1). Its formation in a shallow sea is of interest for this study as the layer of seawater is known to affect the excavation process and the ejecta emplacement (e.g. Shuvalov et al., 2005; Ormö and Lindström, 2000; Lindström et al., 2005b). The Lockne crater is a reference example of the concentric crater morphology obtained when the target is made up of a weak, low-density layer with a thickness equal to about the projectile diameter. Thus, the Lockne crater has a 7.5km wide, deeper, inner crater developed in the crystalline basement surrounded by a 3.5km wide brim where the crater excavation removed most of the 80m sedimentary cover rocks (mainly 50m of limestone covering 30m of dark shale) and 500m of seawater before it was covered by the ejecta flap from the basement crater (Lindström et al., 2005a). The result was a soup-plate-like crater with a smaller, nested crater surrounded by a wider (approximately 14km in diameter) outer crater. The crystalline rocks of the basement are mainly Proterozoic granitoids, but some, somewhat older, metavolcanites occur at the southern part of the crater. The basement target rocks also include several tens of meters thick and hundreds of meters wide, near horizontal dolerite sills that are of special interest to this study.

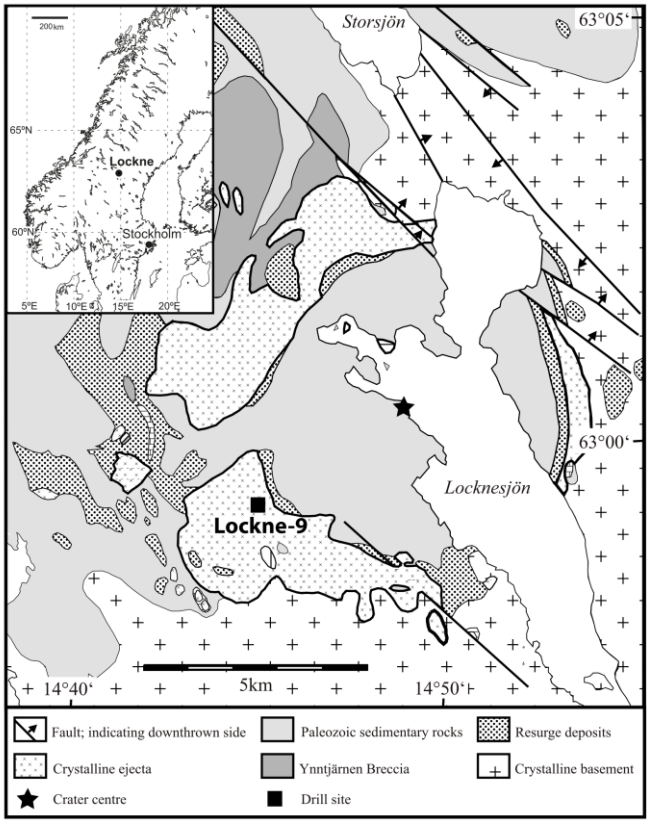

Figure 1. Geological map and location of Lockne-9 drill core with respect to the proposed crater centre (modified after Frisk and Ormö, 2007).

Numerical modeling by Lindström et al., (2005b) describe Lockne as formed by an oblique impact (45º from the East), which caused the outer crater to extend a couple of km further on the down-range side than on the up-range side.

The Lockne crater is today one of the best accessible well-preserved craters on Earth because of the fact that it was covered by post-impact marine sediments and later on also Caledonian nappes (Lindström et al., 2005a). Tertiary isostatic uplift and Quaternary glaciations have allowed erosion to once again expose the crater. This fortunate circumstance has triggered many geological and geophysical studies during the last decades spanning the pre-impact sedimentary record, impact process, and post-impact sedimentation (See Sturkell, 1998a; Lindström et al., 2005a; Ormö et al., 2010, Sturkell et al., 2013, and references therein). The geophysical studies that have been carried out include the modeling of the gravimetric anomaly (Sturkell et al., 1998) and magnetic modeling based on aeromagnetic data (Sturkell and Ormö, 1998). The magnetic modeling was restricted to the use of aeromagnetic anomalies and measured values of the induced magnetization (i.e. magnetic susceptibility) for the geological bodies in consideration. Remanent magnetization as a contribution to the total signal was ignored for simplicity based on scientific argumentation.

The scientific objective with the 2004 Lockne-9 core drilling into the crystalline crater brim and ejecta flap on the western, down-range, side of the crater (Figure 1) concerned the features and the formation process of the ejecta flap. As a consequence of the 45º oblique impact through the layered target (Lindström et al. 2005a,b), a more pronounced flap on the down-range side of the structure was developed. However, until now the only peer-reviewed journal publication in addition to brief and descriptive conference abstracts (e.g., Ormö and Lindström, 2005) is that of Lindgren et al. (2007) dealing with biomineralizations within certain levels of the core. This gives us reason to return to the original objective, but here with a petrophysical approach. Thus, the main objective of this study is to provide a precise analysis of the rock magnetic properties from the 31.04m long Lockne-9 core and use the results in order to analyze the flap formation process.

A comprehensive survey was carried out including i) estimation about the flap thickness to provide information for further estimations of the energy lost during the impact formation and ii) degree of alteration and/or brecciation.

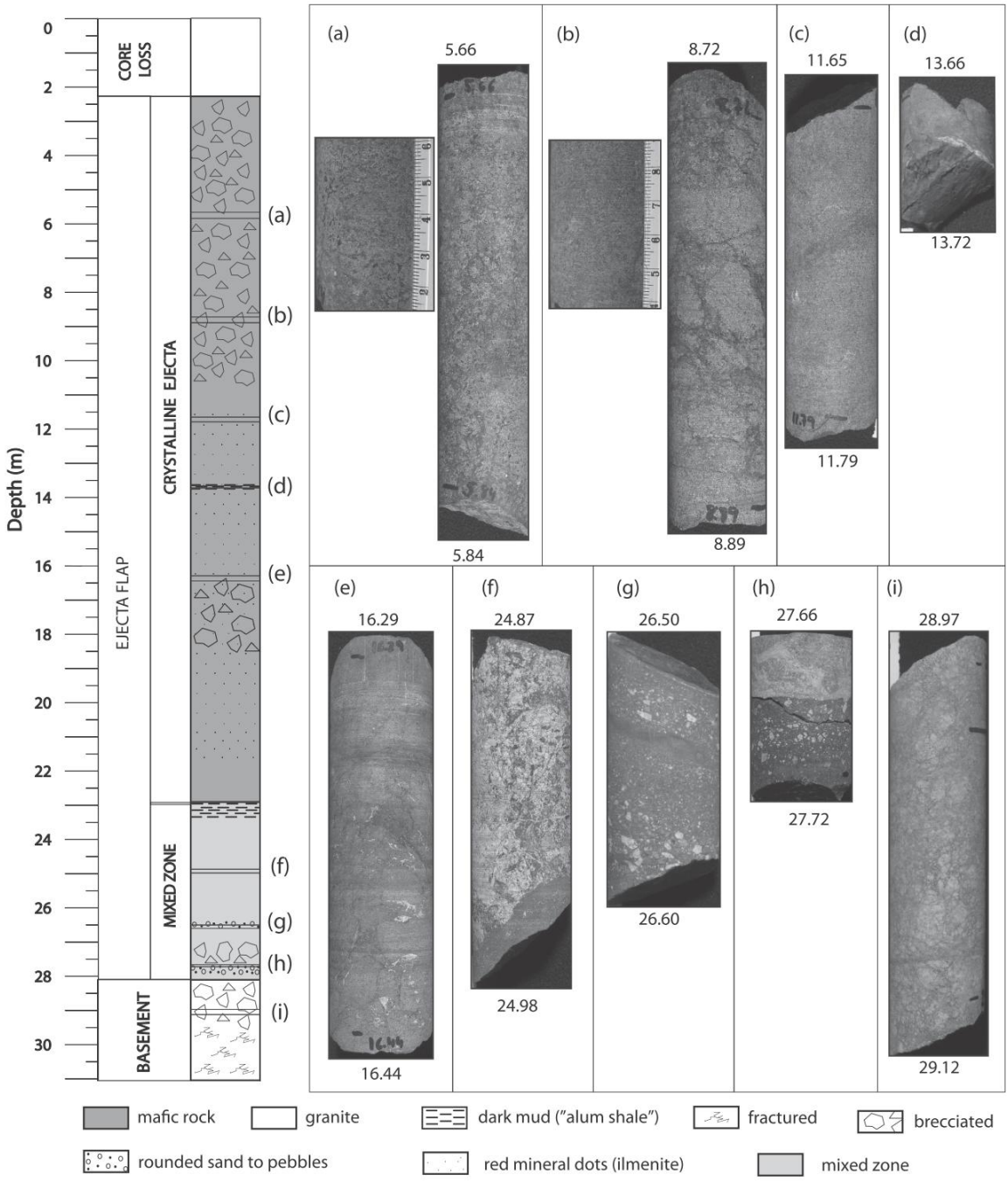

Figure 2. Core log of the Lockne-9 drill core with fotos of representative lithologies discussed in the text.

2. Methodology

Laboratory measurements of rock-magnetic properties were made on samples of different lithologies of the Lockne-9 core. This core was drilled under supervision by Ormö in 2004 and is now stored at the Planetary Geology Laboratory, Centro de Astrobiología (CAB), Spain. Petrophysical measurements were done both at CAB and in the Paleomagnetism Laboratory of the Physics Faculty at the Complutense University, Madrid. Additionally, geochemistry and lithological descriptions have been made to support the interpretations of the petrophysical results, and include X-Ray fluorescence (XRF) spectrometry, thermogravimetric (TGM) analysis and scanning electron microscope micropictures in combination with Energy Dispersive X-ray spectroscopy (SEM-EDX).

2.1. Lithological analysis of the drill core

The original objective with the core drilling was to determine the thickness of the ejecta layer at this down-range section of the Lockne impact structure and to provide information on the shallow excavation flow preceding the ejecta emplacement (Ormö and Lindström, 2005). The 31.04m long and 4.2cm in diameter drill core is nearly complete except for a loss of the uppermost 2.27m. A visual inspection of the Lockne-9 core has been completed with thin sections and SEM-EDX analysis in some selected parts in order to develop a schematic core log to correlate with the magnetic properties obtained during this study.

2.2. Rock magnetism

The magnetic susceptibility of the whole core (425 measurements) was measured in 3-5cm intervals by a SatisGeo KT-6 field kappameter wherever core conditions allowed it (pieces larger than 10cm). In order to reduce the possible external errors because of the bent surface of the cylindrical core, each point was measured three times and an average value was calculated. This susceptibility meter operates at 10kHz frequency and it has a $1 \cdot 10^{-5}$ [SI] sensitivity. A correction factor 2 from the instrument provider was applied for this study attending to the diameter of the core.

A total of 88 chips were cut from the core in order to measure both induced and remanent magnetization in a Coercivity Spectrometer J_Meter (Jasonov et al., 1998). Initial magnetization curves, hysteresis loops, acquisition of Isothermal Remanent Magnetization curves (IRM) and further back-field static demagnetization curves were obtained with this instrument up to a maximum field of 500mT. We have been developed a Matlab routine in order to extract the magnetic parameters out of the Coercivity Spectrometer measurement. A more detailed explanation of the magnetic parameters, their determination and significance can be found in Dunlop and O□zdemir, (1997) and references therein.

The slope of the initial magnetization curves are computed parallel to the specific low-field susceptibility measurements as the susceptibility is dominated by the ferromagnetic minerals. The slope of the hysteresis curve after the saturation of the ferromagnetic phases is called the paramagnetic susceptibility, and it has been measured as a proxy for the identification of changes in the rock matrix.

The hysteresis measurement allowed the determination of the saturation magnetization (M_s), remanent magnetization (M_r) and magnetic coercivity (H_c). Back field curves were used to compute the coercivity of remanence (H_{cr}).

IRM curves help in the identification of the different magnetic fraction depending on the field at which saturation is reached (Butler, 1992). The derivative of the IRM curve can also be used to fully characterize the number and nature of ferromagnetic phases in what has been named as coercivity spectral analysis. There are several methods (Egli, 2004a; Heslop et al., 2002; Kruiver et al., 2001) as well as software to perform that analysis. Because of the simplicity of the initial assumptions we have here chosen the method developed by Kruiver et al., (2001) which it can be used in an Excel spreadsheet. The IRM gradient is fitted into a series of log-normal distributions. The central point of each normal distribution is an indicator of the average coercivity of the population and its standard deviation is an estimation of the uncertain of this property. Each normal distribution with different features indicates fractions with different properties, either due to the same composition but different characteristics, or due to differences in the composition.

Additionally, 36 chips were taken from some chosen samples of every lithology in order to measure thermomagnetic curves up to 700ºC with saturating field of a 1T with the aim of determining the Curie/Neel temperature. These measurements have been carried out in a Variable Force Translation Balance High-sensitivity Magnetometer (VFTB manufactured by Petersen Instruments).

2.3. XRF Spectrometry

The XRF spectrometric analysis was realized in a total of 26 samples from the various lithologies of the Lockne-9 core. This non-destructive technique is based on scattering and quantifying fluorescence radiation generated in the samples as a consequence of the incidence of a beam of X-ray photons (Bertin, 1975). The samples were analysed in a wavelength dispersive sequential X-ray spectrometer PHILIPS PW2404 at the University of Oviedo (Spain). In this study, we have considered the content of SiO_2 as an indicator of diamagnetic materials presence and Fe_2O_3 and Ti_2O as indicators of the magnetic behaviour within the different lithologies of the Lockne-9 core. The percentage of these

main elements measured in samples from Lockne-9 core can be related with the magnetic parameters resulting from the rock magnetic analysis.

3. Results

3.1. Core log description

Based on visual inspection of the core, and to facilitate the comparison with the petrophysical results, we have divided the core into three main lithological sections; the crystalline ejecta, a zone of mixing between ejecta and preserved parts of the target (both forming the ejecta flap), and the autochthonous basement (Figure 2).

3.1.1. *Ejecta flap*

3.1.1.1. Crystalline ejecta

The crystalline ejecta in the core consists mainly of a brecciated, dark grey, mafic rock, which in the upper 11.40m of the breccia is of medium grain size and shows an ophitic texture that gradually disappears downwards. The fragments of the breccia are rotated, angular to subrounded, and occur in a dark matrix. The breccia gets increasingly matrix supported downwards, and in some parts clasts present very good fitting. The clast size varies from a few millimeters up to 3-4dm with dominance of the larger fraction (**Error! Reference source not found.**b). The ophitic texture of the clasts also shows frequent millimeter size black minerals (likely pyroxene) that decrease in frequency to 8m depth (Figure 2a, magnified picture).

At around 11.40m depth a transition to a more fine grained, dark, greenish mafic rock occurs. This part of the core shows a microbreccia with clasts size of about 0.5-2cm (**Error! Reference source not found.**c). Even brecciated larger clasts occur giving the impression of a “breccia in breccia”. Common sub-millimeter size dots of a red mineral appear at 11.70m and with increasing amount downwards in the core until they disappear at 21.80m (**Error! Reference source not found.**c, magnified picture). Our SEM-EDX analysis gave that they are ilmenite. The ilmenite growth seems to be secondary as it overprints the microbreccia. The generally dark matrix passes into dark shale between 13.60m and 13.72m (**Error! Reference source not found.**d). Its origin from the Cambrian alum shale is inferred from its U-Th rich bitumen nodules observed by Lindgren et al. (2007). Hence, it can be assumed some of the dark matrix of the breccia has the same origin. The micro-breccia is most obvious in the transitional part, from 11.40m, to the coarser rock (up to 14.40m). Below this interval of the core, the greenish mafic rock gets very fine grained and any brecciation is hard to distinguish, although some disintegration is visible between 16.30m and 18.80m, again possibly a secondary brecciation of a solidified breccia (**Error!**

Reference source not found.e). From 18.80m downward, the material is again more obvious clast supported breccia with subrounded clasts with sizes up to a couple of centimeter within a fine grained, black matrix.

3.1.1.2. Mixed zone

Sandwiched between the mainly mafic crystalline ejecta and the granitic basement is a mixed zone of both mafic and granitic breccia clasts blended with sediments from the Palaeozoic target sequence. This mixed zone begins at 22.90m depth with 50cm of dark mudstone (i.e., Cambrian alum shale). It is followed downwards by a granitic breccia between 23.40m and 26.40m, (**Error! Reference source not found.**f). The clasts are angular with good fitting. Some well-rounded crystalline pebbles occur in the otherwise black matrix. Thus it is reasonable to assume a provenance from the Lower Cambrian conglomerate of the target succession. At 26.40m there is a 20cm thick section of dark matrix that show fractioning of the grain sizes from silt at the contacts to the surrounding breccia blocks to gravel in its central part (**Error! Reference source not found.**g). The dark mud and the pale, weathered, fragments in the coarser fraction suggest a provenance from the Cambrian conglomerate. However, the size sorting indicate emplacement as an injection (cf. injected dikes described by Sturkell and Ormö 1997). The core continues downwards with a blend of granitic breccia, often with dark matrix, and dm-thick sections of alum shale. In **Error! Reference source not found.**h the contact between clast supported, granitic breccia (top) at 27m depth and 22cm of reworked Lower Cambrian conglomerate (bottom) is displayed. It shows similarities to the occurrence shown in **Error! Reference source not found.**g at 27.67m depth.

3.1.2. Basement

The breccias and reworked sediments of the ejecta and the mixed zone rest with a sharp boundary at 28.10m depth on fractured and brecciated basement. This depth coincides with the estimated level of the sub-Cambrian peneplain (Ormö and Lindström, 2005 and Sturkell and Lindström, 2004). The dominantly light grey granitic rock of the basement is in stark contrast to the overlying mafic rocks of the ejecta and continues to the end of the core at 31.04m depth. The basement is strongly brecciated (**Error! Reference source not found.**i), mostly clast-supported with good fitting, but locally matrix-supported with rotated clasts of a few millimeters up to a decimeter in size in a dark matrix.

3.2. Rock magnetism-bulk properties

Error! Reference source not found. shows histograms that summarize the measured susceptibility values. The highest susceptibility values are observed in the crystalline ejecta, corresponding to the mafic rock. The peak value is $58.2 \cdot 10^{-3}$[SI] to be compared with the minimum value of $-0.10 \cdot 10^{-3}$[SI] measured in the granitic fractured and brecciated basement (Figure 3a and Figure 3d). Thus, there is a clear difference between the crystalline material of the ejecta flap and the basement. Obtained values correlate well with previous measurements in corresponding lithologies in the Lockne impact crater (Törnberg and Sturkell, 2005). The crystalline ejecta low field susceptibility follows a bimodal distribution of values, with a narrow population with values in the order of 10^{-3}[SI] and a second population of higher susceptibility and wider (Figure 3b). This second population has magnetic susceptibility values between $1.6 \cdot 10^{-2}$[SI] and $4.4 \cdot 10^{-2}$[SI], which means two or three orders of magnitude higher than the rest of the core. The mixed zone has a well-constrained susceptibility in the order of 10^{-4}[SI] (**Error! Reference source not found.**c). Negative susceptibility values occur for material from the fractured and brecciated granitic basement and may correspond to a diamagnetic material, most likely due to high abundance of quartz content (Figure 3d).

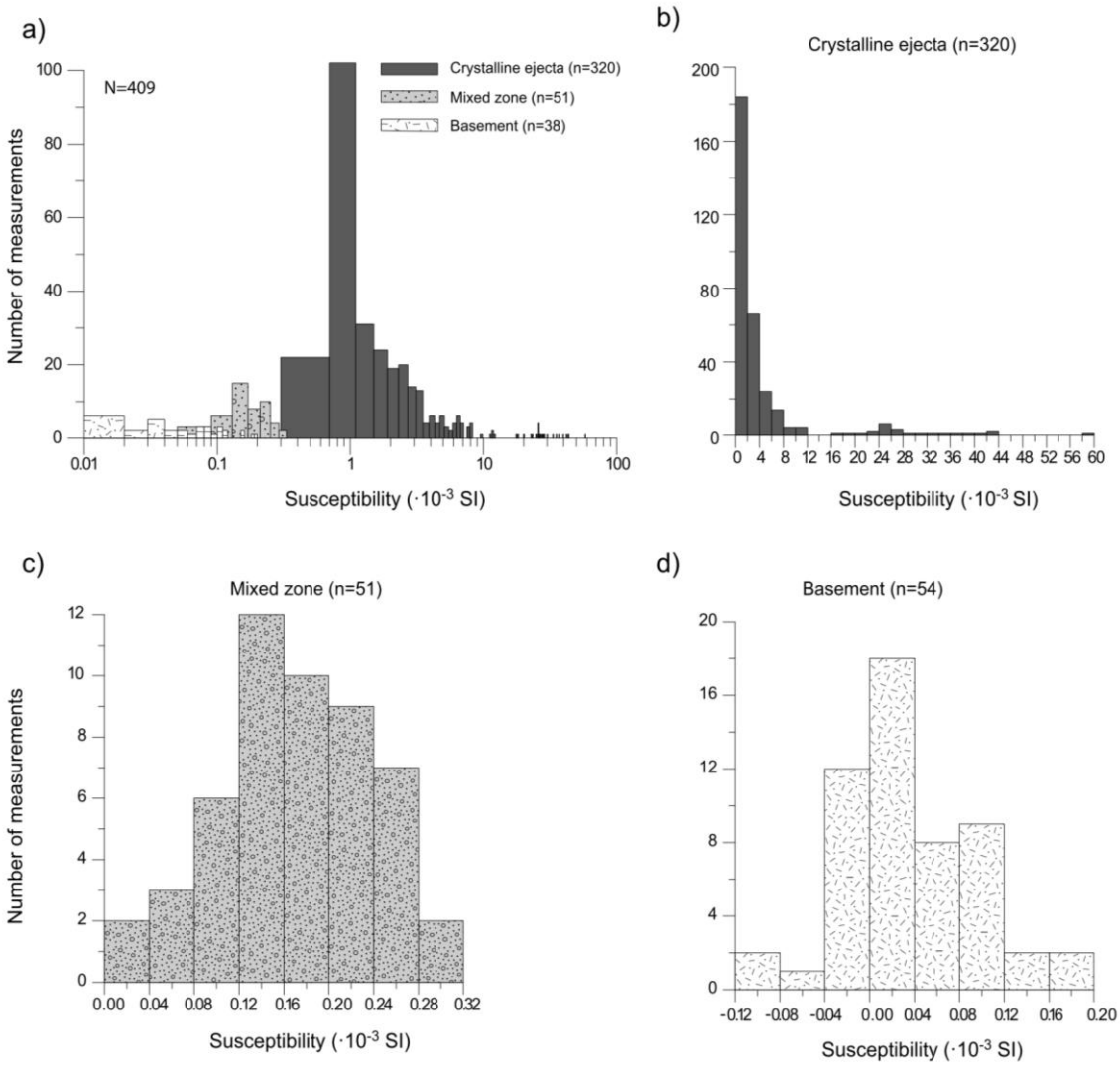

Figure 3. Histograms of magnetic susceptibility obtained with a KT-6 hand susceptometer for the three main lithological sections of the Lockne-9 core: a) a logarithmic histogram comparing the three major lithologies. In the logarithmic histogram 14 negative or zero values had to be removed by the logarithm definition, b) Crystalline ejecta, c) Mixed zone, and d) Fractured basement.

We observed three different types of hysteresis loops depending on the main carrier of the magnetic signal: i) practically dominated by the paramagnetic fraction, ii) dominated by the ferromagnetic phases or iii) mixed by the two types of magnetic minerals (**Error! Reference source not found.**). The upper part of the core displays a mixed composition, with a significant paramagnetic contribution to the magnetization curve and a closed hysteresis loop (Figure 4a). After substraction of the paramagnetic signal, the hysteresis reaches saturation at approximately 250mT and displays an open loop with coercivities between approximately 17 and 92mT.

The hysteresis loops dominated by the ferromagnetic fraction are found mainly in the upper part of the transition to the more fine grained, greenish, mafic rock in the ejecta flap (between 11.40 and 12.50m) with almost no contribution of the paramagnetic fraction

(**Error! Reference source not found.**b). The bottom part of the core, from 22.90m to the end, corresponding to the mixed zone (Figure 4c) and the basement (Figure 4d), is dominated by the paramagnetic / diamagnetic fraction. After the paramagnetic correction the hysteresis loops show an almost closed loop with very low coercivity (Dunlop and O□zdemir, 1997). Therefore, magnetic susceptibilty derived from hysteresis loops is consistent with values already obtained by direct low-field susceptibility measurements. In all analyzed samples the hysteresis loop reaches saturation at 250mT, although the saturation magnetization vary depending on the lithology. The obtained values of coercivity and the field at which saturation is reached suggest the presence of magnetite/titanomagnetite (Dunlop and O□zdemir, 1997).

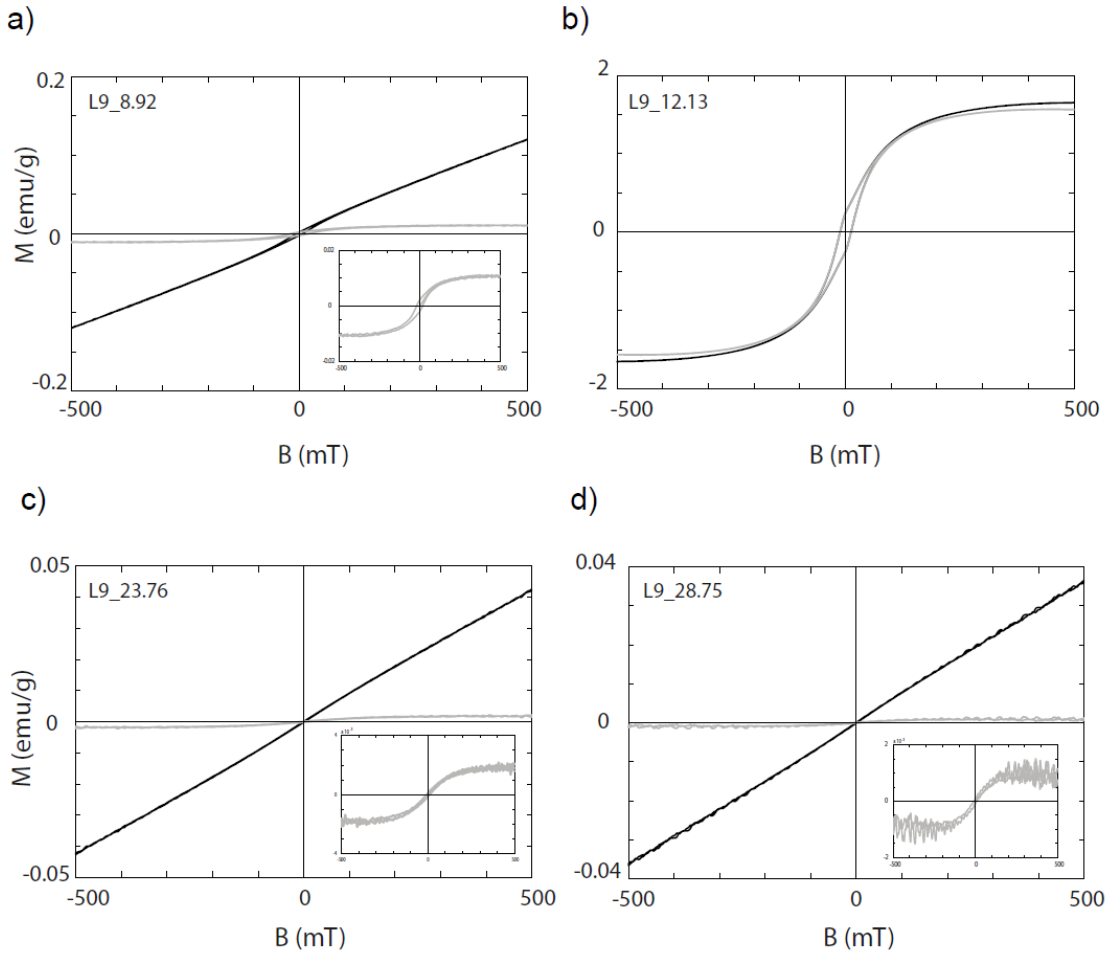

Figure 4. Typical hysteresis loops obtained from the three main lithologies in the Lockne-9 core. The black curve represents the measured hysteresis and the grey curve represents the hysteresis corrected by the paramagnetic susceptibility. The inset shows a magnified part of the corrected hysteresis loop. Graphs a) and b) represent loops obtained from the crystalline ejecta flap, graph c) shows typical loops for the mixed zone and graph d) shows loops for the granitic basement. Graph a) shows mixed loops with contribution from both paramagnetic and ferromagnetic fraction, graph b) shows loops dominated by the ferromagnetic fraction and c) and d) show loops dominated by the paramagnetic fraction.

Three typical types of IRM acquisition curves have been obtained along the core (**Error! Reference source not found.**). Saturation is reached in samples with the type of curves represented by Figure 5a at about 250mT. This result suggests the presence of magnetite/titanomagnetite in these type of samples (Lowrie, 1990) . Several samples show a different behavior with saturation that is not reached at 500mT (**Error! Reference source not found.**b). The high coercivity suggests the presence of a high coercivity mineral, most commonly goethite or hematite (Lowrie, 1990). The rest of the samples show a mixed curve with a fraction suturing at 250mT and another fraction that not reaches saturation (**Error! Reference source not found.**c and d).

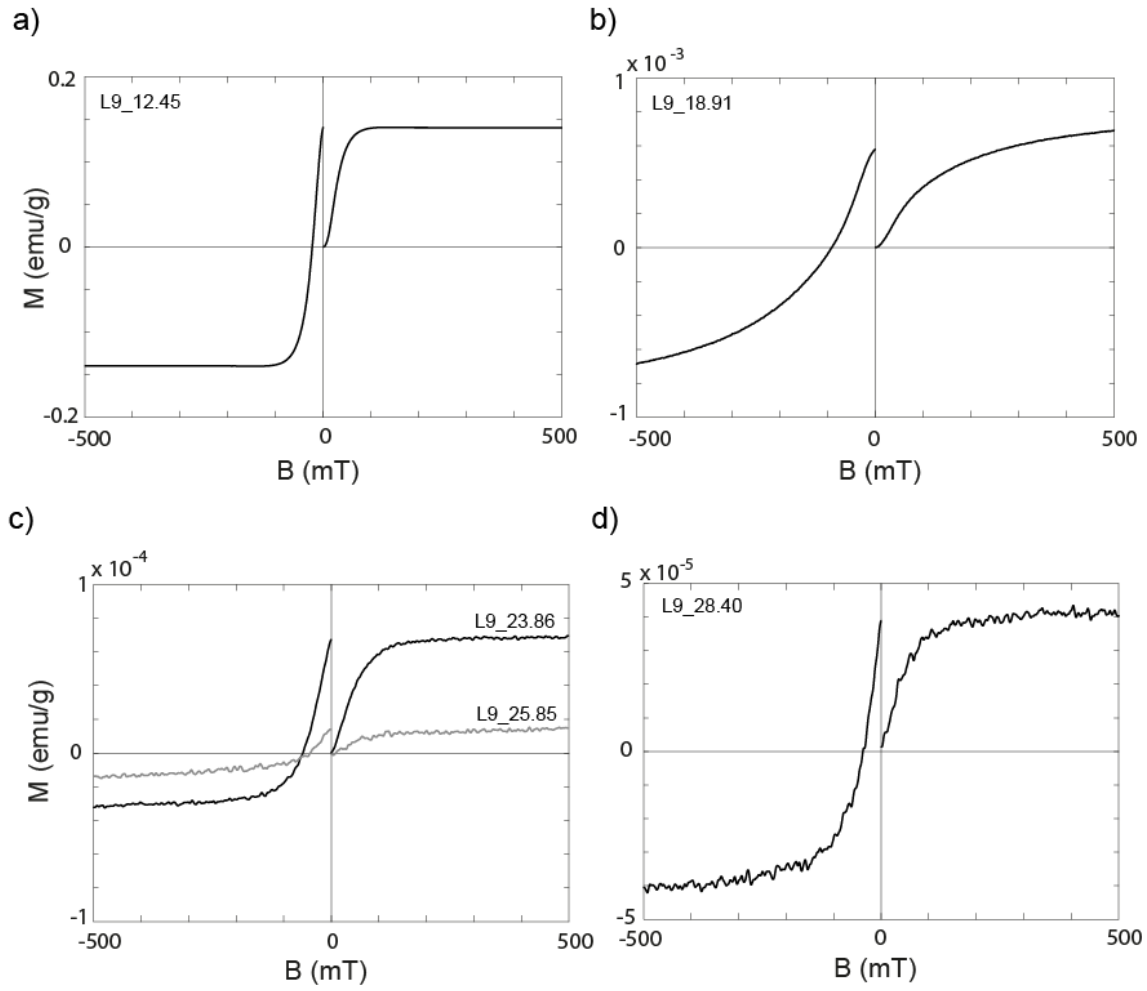

Figure 5. Typical IRM acquisition and back field demagnetization curves from the different lithologies of Lockne-9 core. Graphs a) and b) show curves obtained for the crystalline flap, c) shows two curves represented in black and pale grey obtained for the mixed zone and d) shows a curve obtained for the granitic basement. a) and c) (black curve) show IRM curves reaching saturation at 250 mT approximately, b) shows an IRM curve that did not reach saturation for the maximum field applied, and c) (pale grey) and d) show mixed curves with contribution from a fraction that reached saturation at 250 mT and one that did not reach saturation.

The coercivity spectra of a total of 36 characteristic samples were analyzed following the protocol described by Kruiver et al. (2001), and is displayed in three selected characteristic curves in **Error! Reference source not found.**. 24 samples display an IRM acquisition curve dominated by one population of magnetic minerals and, therefore, the corresponding coercivity spectra is also dominated by one main function (Figure 6a and Figure 6c). This spectrum has a main normal distribution centered at 1,50mT and with a 0.25 dispersion parameter value, which is the main carrier of the signal. This type of IRM coercivity spectra is observed mainly in the crystalline ejecta. Additionally, it has been necessary to include one population with low median destructive field ($B_{1/2}$ = 10mT) and a dispersion parameter (DP = 0.28) that contributes less than 15% of the signal. Some authors have attributed this to thermal activation processes of the magnetic particles (e.g., Heslop et al., 2004). In some samples of this type, at high coercivities also a minor distribution has been included that contributed less than a 5%, which is considered a mathematical artifact due to the instrumental noise at high fields. 12 samples displayed an IRM acquisition curve that did not saturate at 500mT. The corresponding coercivity was fitted into a distribution with two different components of similar intensity (Figure 6b). This high coercivity population contributes to 20-64% of the signal depending on the sample, with high median destructive field of $B_{1/2}$= 501.2mT and a dispersion parameter DP=0.45. Moreover, is necessary to include the low coercivity population attributed to the thermal activation process of the particles.

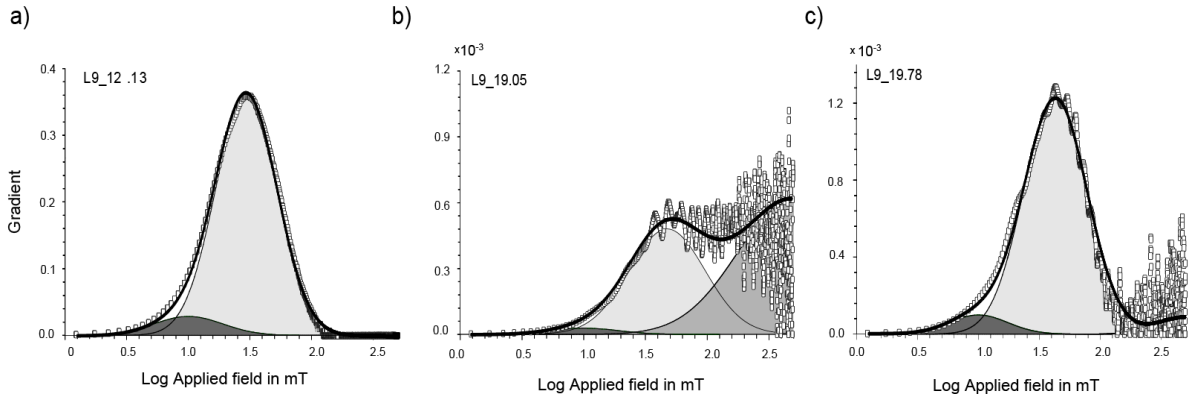

Figure 6. Derivatives of the IRM curves (white symbols) with the corresponding modeled curve derived from the fitting into a series of gaussian distribution of coercivity-derived curves (thickest black curve). Individual components of the different magnetic fractions and coercivity distributions are shown as grey shadowed areas for the three examples.

A summary of the domain state can be visualized in a so-called Day plot, proposed initially by Day et al. (1977). The coercivity ratios as function of the magnetization ratios are a proxy of the domain state depending on the area of the plot where the data lay. The ratios were described later as a mixture of two endmembers of single domain (SD) and multidomain

(MD) particles giving rise to theoretical mixture curves (Dunlop, 2002a) . **Error! Reference source not found.** shows that several samples from the crystalline ejecta are inside the Day pseudo-single domain zone (PSD) and it corresponds to a mixture with 50% from single domain and 50% from pseudo-single domain obtained by Dunlop (Dunlop and O□zdemir, 1997). A gradual increase to the MD zone with depth is observed with the exception of the granitic basement that is laying in the boundary between PSD and MD region.

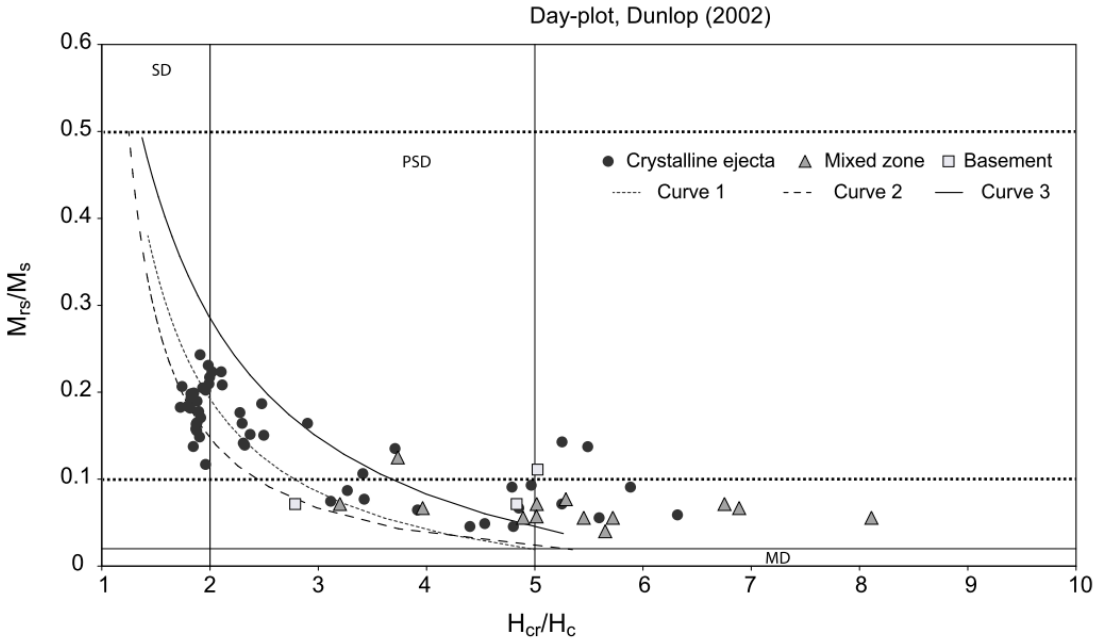

Figure 7. Day plot summarizing magnetization ratios M_{rs}/M_s as a function of coercivity ratios H_{cr}/H_c(Day et al., 1977) for the three studied lithologies where the significance of the symbols appears in the legend. Curves 1, 2 and 3 correspond to mixture models proposed by (Dunlop, 2002).

Thermomagnetic curves have been analyzed for 35 samples from the drill core. Since thermal methods lead to the destruction of the material only representative samples have been measured. The Curie temperature of the ferromagnetic phases has been obtained using the second derivative methods (Moskowitz, 1981). **Error! Reference source not found.**a shows a characteristic thermomagnetic curve obtained from samples located in the crystalline ejecta. The heating curve indicates a first inflexion of the curve around 100ºC, and the cooling curve presents a second Curie temperature value around 525ºC that could be attributed to the titanomagnetite with a low Ti content (O'Reilly, 1976). The upper part of the transition to the more fine greenish mafic rock, between 11.40 and 12.50m, is evident in the thermomagnetic curves (**Error! Reference source not found.**b). For these samples the heating curve indicates an initial presence of a ferromagnetic fraction, and the cooling curve reveals a Curie temperature around 580ºC corresponding to magnetite (Dunlop and

O□zdemir, 1997). The cooling curve in **Error! Reference source not found.**b shows an initial part of total overlap revealing a reversible behavior, and the following higher demagnetization temperature indicates slight alteration of the initial features. **Error! Reference source not found.**c shows the two different types of thermomagnetic curves obtained from the mixed zone. The thicker lines represent samples where the heating measurements shows an unblocking temperature around 100ºC and a local maximum centered on 500ºC, which indicate the presence of an important paramagnetic fraction of pyrite. On the other hand, the thinner lines from **Error! Reference source not found.**c as well as the **Error! Reference source not found.**d (that represents samples from the fractured and brecciated basement) show thermomagnetic curves where both heating and cooling curves are very noisy and the diamagnetic/paramagnetic materials dominates the magnetic signal.

Many of the thermomagnetic curves analyzed from the ejecta flap present a decrease in the magnetization of the heating curve around 100ºC (Figure 8a and c). When this inflexion is related to the unblocking temperature of a ferromagnetic phase, the most likely mineral to support this hypothesis would be goethite. It has a Curie temperature of 120ºC that can be decreased by a number of factors such as low crystallinity, stoichiometry, higher water content or inclusion such as Al (Dekkers, 1988). In order to corroborate the presence of goethite, additional thermogravimetric analyses (TGA) have been carried out in six significant samples (see complementary material) finding no insignes of goethite dehydroxylation in the weight or heat loss flow with temperature. These analyses conclude that goethite is not present in these samples.

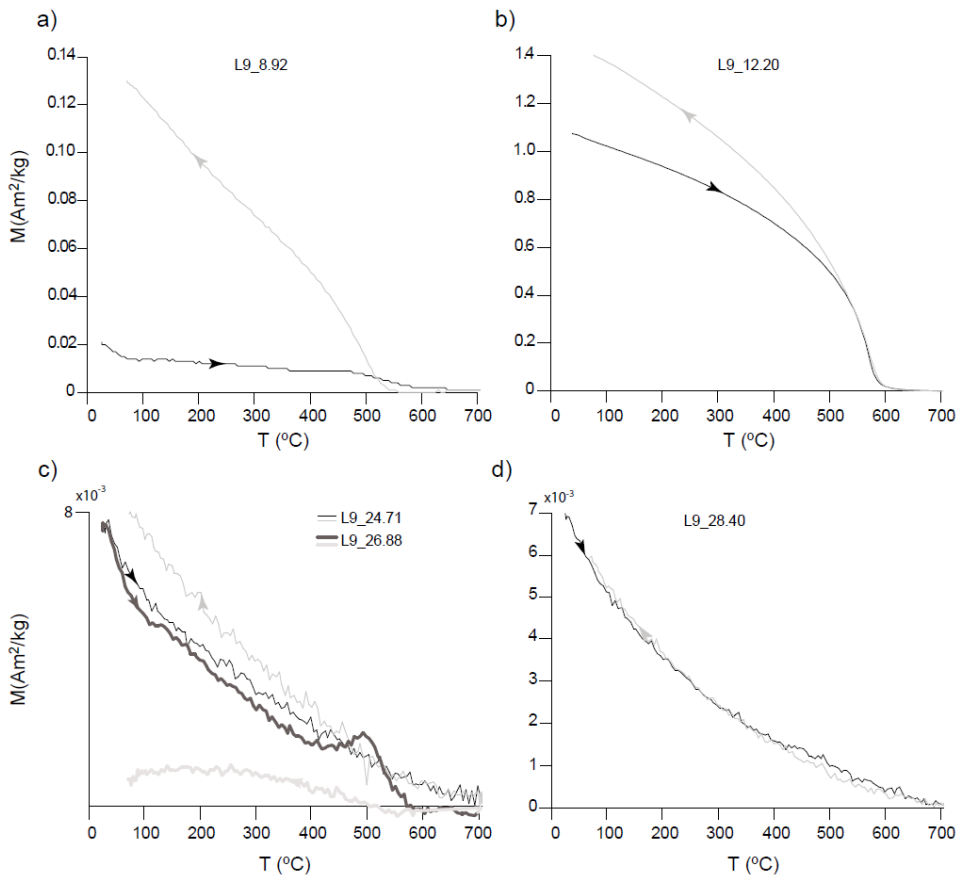

Figure 8. Characteristic thermomagnetic curves obtained from the three main lithologies of Lockne-9 core where black indicates the heating curve and pale grey indicates the cooling measurements. Graphs a) and b) show thermomagnetic curves obtained for the crystalline ejecta flap, c) shows two representative curves obtained for the mixed zone, and d) shows thermomagnetic curves for the granitic basement.

3.3. Rock–magnetism profiles

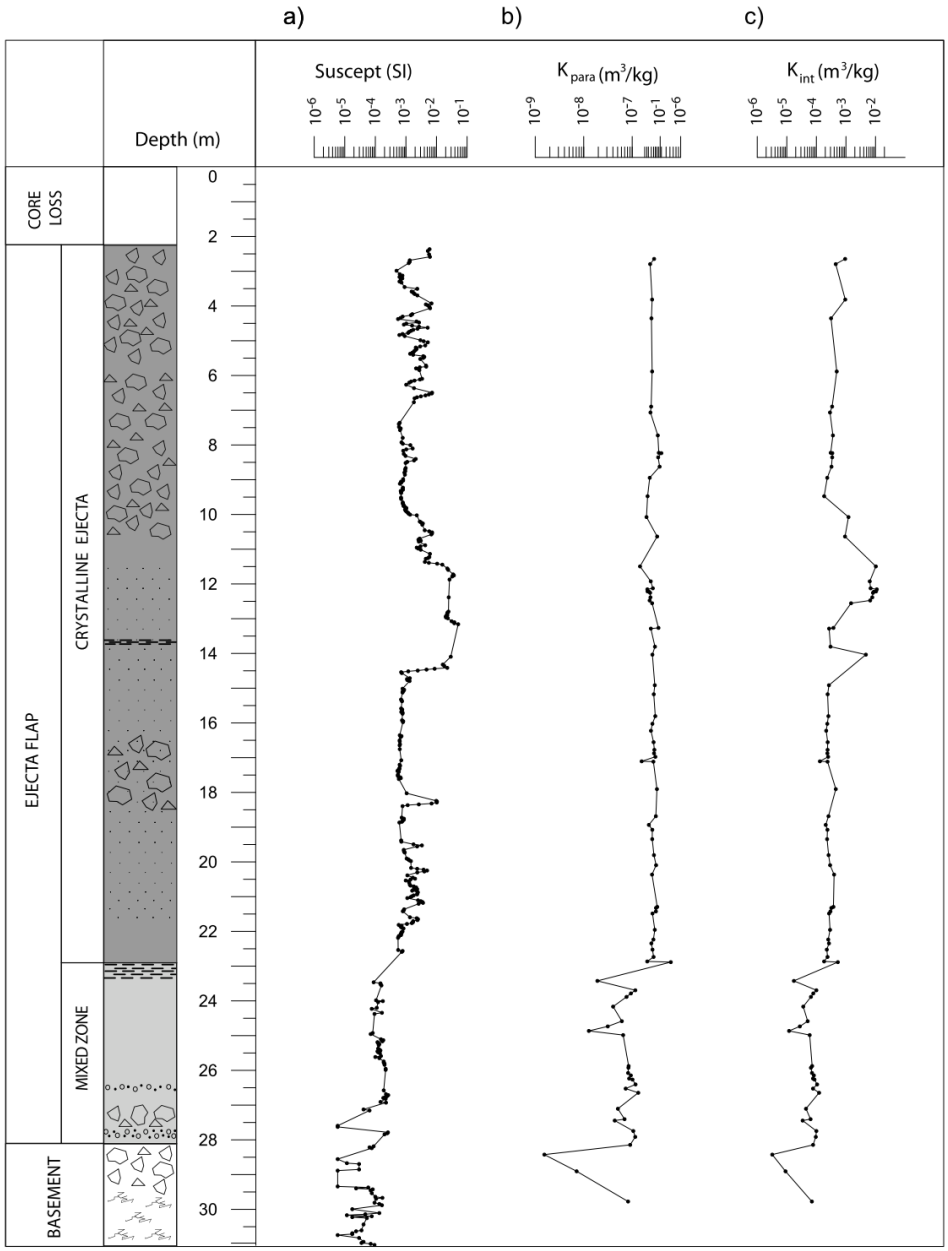

Figure 9. Representation of the dependence of the different susceptibility results obtained by different methods along the Lockne-9 drill core. Graph a) shows paramagnetic susceptibility obtained from the coercivity spectrometer (J_Meter) measurements, b) initial susceptibility obtained from the coercivity spectrometer (J_Meter) measurements, c) susceptibility measurements obtained with a KT-6 field susceptimeter.

Error! Reference source not found. shows a summary of magnetic susceptibility as a function of depth. **Error! Reference source not found.Error! Reference source not found.**a represents the low-field susceptibility measured with the KT-6 field kappameter along the whole core, previously represented in histograms in Figure 3. Values are very similar along the profile with the exception of levels between 11.40 and 14.40m approximately, which coincides with the transition to the more fine grained greenish variety of the mafic rock. As the susceptibility histograms have shown before, a decrease in

susceptibility values within the mixed zone and the basement is very clear. Paramagnetic susceptibility computed as the slope of the hysteresis loop above saturation of the ferromagnetic phases can be seen in **Error! Reference source not found.**b. Samples from the crystalline ejecta hardly show any variations of paramagnetic susceptibility as a function of depth. This indicates a homogeneous composition within this lithology. A very clear decrease in paramagnetic susceptibility is observed in the mixed zone and the fractured basement as a consequence of an increasing content of granite. The fractured basement shows low values close to the diamagnetic boundary. **Error! Reference source not found.**c shows the initial susceptibility profile calculated as the slope of the initial magnetization at low values of the field. The initial susceptibility is mainly due to the ferromagnetic minerals. The signal is very homogeneous along the profile with the exception of a maximum between 11.40m and 14.40m. This zone correlates to the maximum observed in the bulk susceptibility profile (**Error! Reference source not found.**a) and corresponds to the transition to the more fine grained greenish variety of the mafic rock. These profiles suggest that this part of the crystalline ejecta present an increase of the ferromagnetic content. Comparing the content of the major elements from Table 1, there is not obvious difference in values within the crystalline ejecta lithology although highest values of Ti have found in this transition zone.

Table 1. Major elements content from Lockne-9 core samples.

Depth (m)	Si (%)	Fe (%)	Ti (%)	Al (%)	Ca (%)	Mn (%)	K (%)	Mg (%)	Na (%)	P (%)
4.33	42.13	15.92	1.99	14.45	5.47	0.31	1.18	9.91	1.67	0.23
7.70	40.80	16.38	2.20	13.73	4.91	0.32	0.84	10.81	1.72	0.24
8.60	38.93	14.26	1.34	13.22	10.01	0.27	0.60	9.35	1.44	0.17
10.61	41.84	15.65	1.91	10.75	7.68	0.25	0.55	9.88	1.24	0.26
12.30	**45.38**	**14.57**	**2.22**	**16.65**	**2.68**	**0.16**	**2.59**	**8.47**	**1.87**	**0.25**
12.45	**45.17**	**14.58**	**2.24**	**16.73**	**2.34**	**0.18**	**3.50**	**8.02**	**1.80**	**0.26**
12.81	**45.59**	**16.47**	**2.67**	**14.57**	**1.73**	**0.17**	**3.79**	**8.34**	**1.63**	**0.33**
13.24	**41.60**	**17.30**	**2.18**	**15.05**	**1.97**	**0.14**	**2.83**	**7.92**	**1.04**	**0.25**
15.22	42.17	13.49	1.93	14.26	8.57	0.19	0.62	9.57	0.26	0.21
15.44	42.09	13.33	1.88	14.02	8.42	0.18	0.63	9.5	0.26	0.21
16.13	44.53	13.52	2.07	15.76	9.32	0.14	0.44	8.08	0.07	0.24
16.53	34.83	14.15	1.90	17.49	8.52	0.17	0.76	12.33	0.05	0.24
18.66	40.81	14.93	2.09	15.96	6.64	0.17	0.38	11.38	0.07	0.28
19.03	47.95	13.77	2.10	15.80	2.17	0.15	2.47	7.31	2.04	0.23
19.05	48.60	13.05	2.13	15.75	1.95	0.14	2.84	7.02	1.90	0.23
20.34	43.40	15.42	2.07	15.70	1.89	0.20	2.59	10.07	1.29	0.27
21.39	42.77	14.46	2.12	16.58	3.08	0.17	3.41	8.57	1.82	0.25
21.43	43.00	12.92	2.13	16.13	4.12	0.15	3.59	7.68	2.02	0.24
22.24	40.22	16.34	2.29	17.51	1.77	0.15	2.30	10.54	1.27	0.26
23.86	54.68	3.96	0.33	19.08	2.55	0.08	3.94	6.40	0.07	0.03
24.71	56.15	3.67	0.24	19.08	2.69	0.08	4.41	6.09	0.08	0.03
26.12	58.49	4.72	0.18	16.64	2.72	0.09	2.92	6.88	0.07	0.06
27.42	64.08	2.69	0.14	15.62	1.60	0.04	5.52	4.00	0.81	0.03
27.89	50.34	6.52	0.52	18.82	2.65	0.10	5.28	7.46	0.44	0.10
28.72	63.39	0.77	0.14	18.77	2.40	0.02	0.45	0.54	10.25	0.03
29.75	59.00	4.23	0.37	18.99	2.25	0.05	5.89	2.76	2.97	0.07

Bold indicates the samples within the high susceptibility zone.

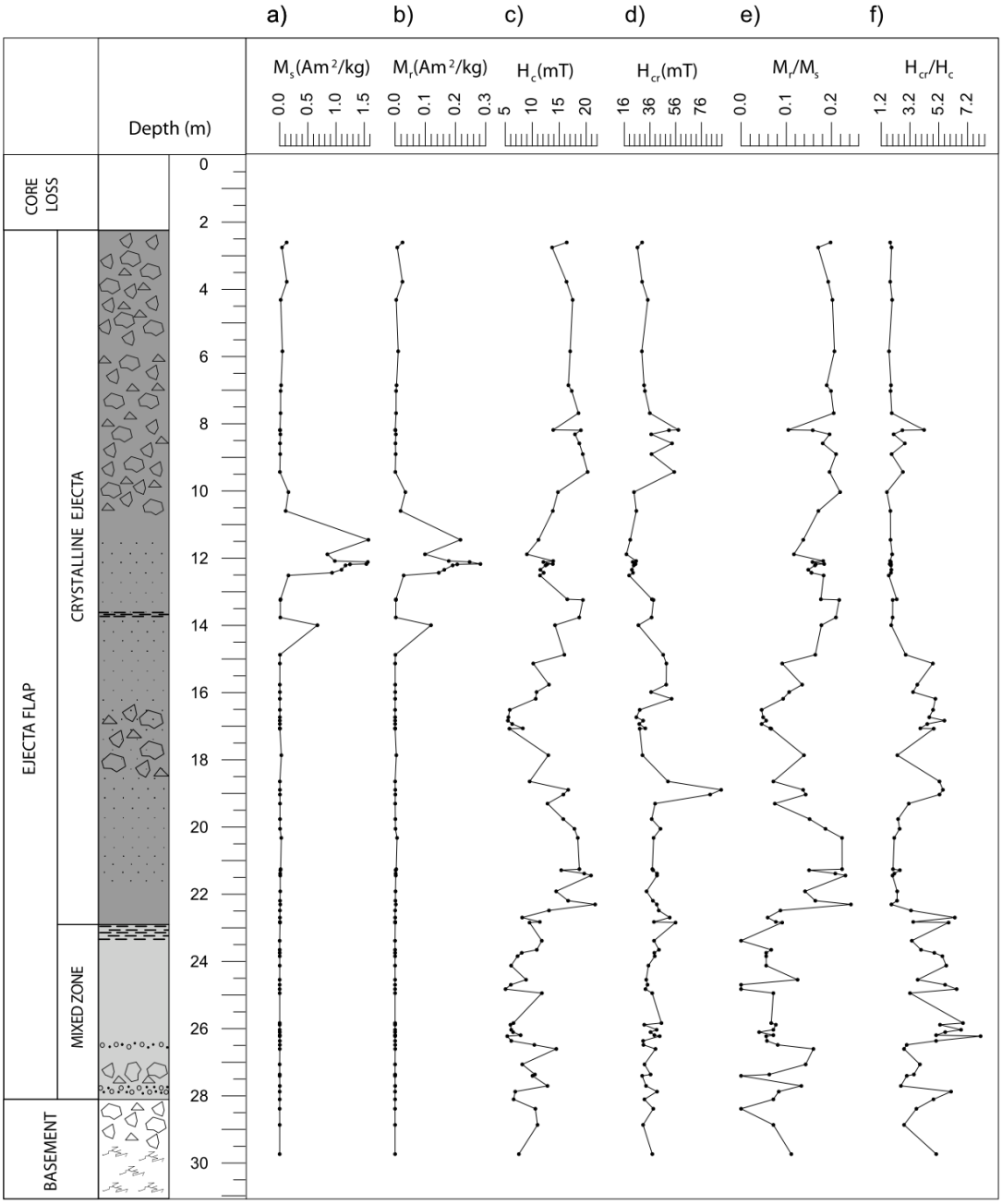

Figure 10. Representation of the dependence of the different magnetization and coercivity results obtained from the coercivity spectrometer (J_Meter) measurements with depth on the Lockne-9 drill core. Graph a) saturation magnetization, b) remanent magnetization, c) magnetic coercivity, d) coercivity of remanence, e) Magnetization ratio M_r/M_s, and f) the coercivity ratio H_c/H_{cr}.

Error! Reference source not found. shows the hysteresis parameters as a function of depth. Magnetization parameters (**Error! Reference source not found.**a and b) have a similar behavior with almost constant values of about $M_s=10^{-2}Am^2/Kg$ and $M_r=10^{-3}Am^2/Kg$ with the exception of the levels between 11.40 and 12.50m where there is an increase in

both parameters. This is a similar behavior as observed in the initial susceptibility (**Error! Reference source not found.**b) and in the bulk susceptibility (**Error! Reference source not found.**c). This happens in the transition to the more fine grained greenish variety of the mafic rock in the ejecta flap. The coercivity parameters (**Error! Reference source not found.**c and d) show a similar trend, and ranges between H_c=5mT and H_c=20mT. Samples from the crystalline ejecta present high coercivity values of about 15mT that decreases downwards reaching a minimum at about 12m. This minimum corresponds to the maximum in M_s and M_r already described. This lithology presents the more complex behavior in terms of coercivity. It has a maximum at 13.26m following by the absolute minimum of the core at 17m and recovers high values of about 21m toward the end of the lithology. The mixed zone and the fractured basement slowly tend towards low values of coercivity. Ratio between M_r and M_s and ratio between H_c and H_{cr} were calculated in order to study its behavior along the Lockne-9 core (**Error! Reference source not found.**e and f respectively). The highest ratios of M_r/M_s have been reached in the flap. A notable decrease is observed along the depth of the core, but in two zones of the crystalline ejecta (between 11 and 15m and between 20 and 22m) high ratios were reached (between 0.20 and 0.24 approximately). At the bottom part of the core, very low values have been obtained. The ratio between H_c and H_{cr} ranges from 1 to 3 along almost the whole crystalline ejecta, but a zone stand out with high ratio between 15 and 19m approximately. This ratio increases in the mixed zone and fractured basement reaching values from 3 to 5. It is important to emphasize the inverse relationship between these two ratios in the main trend and in several little peaks (as the ones observed in 8, 9 and 10m approximately).

3.5. XRF Spectrometry

Major element data have been obtained by XRF technique in a total of 26 samples from the core (**Error! Reference source not found.**). **Error! Reference source not found.Error! Reference source not found.** shows the relations between the most relevant major elements measured: Fe versus Si (**Error! Reference source not found.**a), Ti versus Si (**Error! Reference source not found.**b) and Fe versus Ti (**Error! Reference source not found.**c). Results show a clear grouping of values: group 1 is dominated by the mafic rock of the crystalline ejecta and group 2 is dominated by the mainly felsic rocks of the mixed zone and the fractured basement. Samples belonging to group 1 present low Si and higher Fe and Ti. Opposite behavior is observed in samples from group 2 with higher Si and lower Fe and Ti.

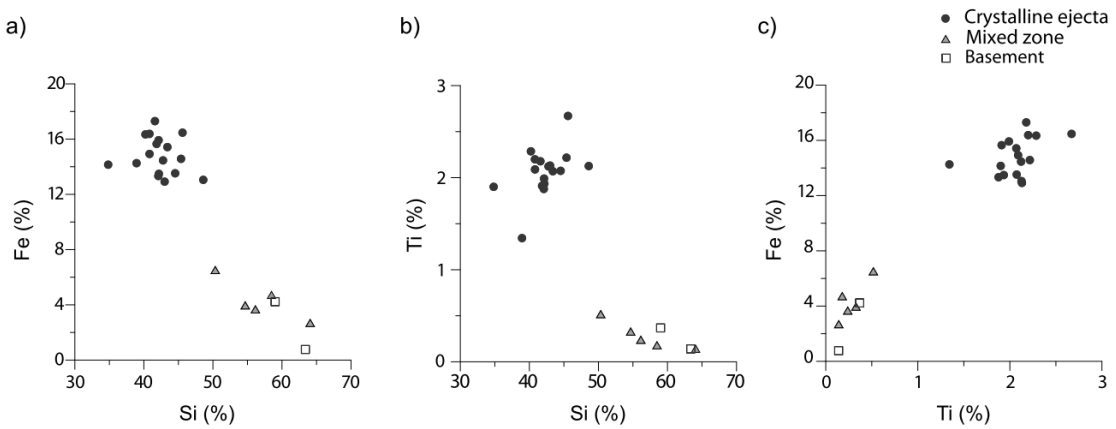

Figure 11. Representation of the relations between the content of the most relevant major elements. a) Fe vs. Si, b) Ti vs. Si, and c) Fe vs. Ti content of 25 samples from the Lockne-9 core. Each symbol represents a different lithology (see legend).

Error! Reference source not found. shows the relations between the most relevant major elements and some of the magnetic parameters obtained by the rock magnetic analysis described above. **Error! Reference source not found.**a, b and c represent the relationship between the paramagnetic susceptibility and the Si, Fe and Ti content respectively. The same grouping is found in this plot. High paramagnetic susceptibility is observed in samples from group 1 together with high Fe and Ti contents suggesting that Fe and Ti are present within the lattice of paramagnetic minerals (cf. Rochette, 1987) (**Error! Reference source not found.**b and c).

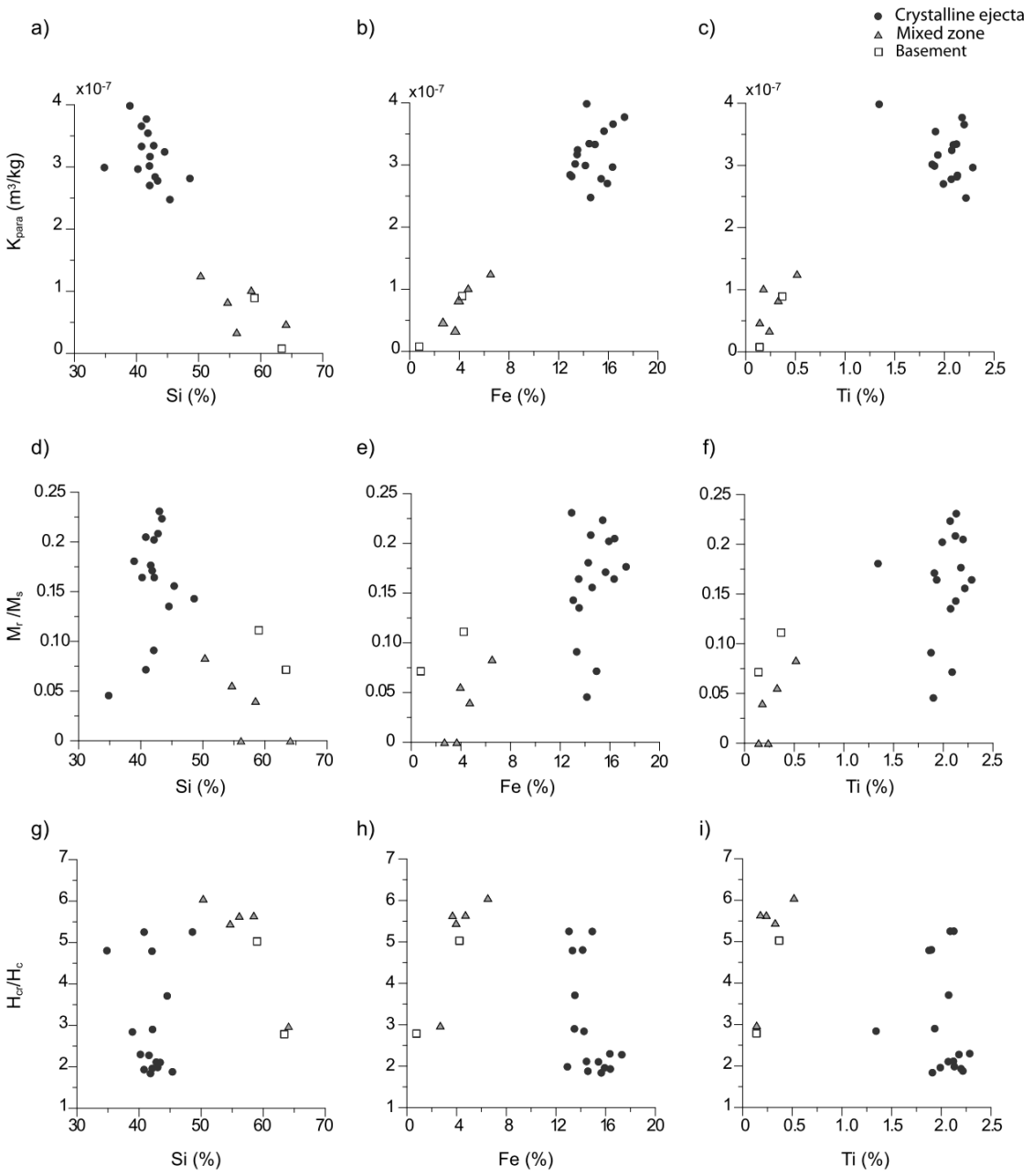

Figure 12. Representation of the dependence of the most relevant major elements to different magnetic parameters. Paramagnetic susceptibility vs. : a) Si, b) Fe and c) Ti content; magnetization ratio, M_r/M_s vs : d) Si, e) Fe and f) Ti content and coercivity ratio, H_{cr}/H_c vs: g) Si, h) Fe and i) Ti content.

The relationship between these elements contents and the ratio between M_s and M_r is shown in **Error! Reference source not found.**d, e and f. The distinction of the two main lithological groups is also observed in these plots. The same type of behavior as observed in the paramagnetic susceptibility is seen also for the ratio M_s/M_r in relation to the Si, Fe and Ti content. However, three samples from the ejecta flap show lower magnetization ratios. These samples correspond to singular minimum peaks observed between 15 and 19m

depth in **Error! Reference source not found.**e. **Error! Reference source not found.**g-i show the relation between the ratio H_{cr}/H_c and the Si, Fe and Ti content. The coercivity ratio is a less sensitive parameter to the cation content in this case, and the general classification in two groups cannot be applied.

3.4. Comparative data

We have compared the measurements from the high magnetization zone obtained from the rock magnetic study in Lockne-9 core (from 11.40 to 12.50m) with three samples extracted from different dolerite outcrops unaffected by the impact and carried out similar rock magnetic experiments (**Error! Reference source not found.** and Table 2). Comparison of the coercivity spectral analysis reveals a similar behavior of both affected and unaffected samples by the impact with a slight hardening of coercivity of the second (Figure 13a). This property is also observed in the higher values of the median destructive field when compared with the SIRM (Figure 13b). The Day plots of both types of samples are grouped in the same area although the coercivity ratio is lower in the unaffected dolerite (**Error! Reference source not found.**c). Thermomagnetic curves represented in **Error! Reference source not found.**d reveal a unique unblocking temperature for all the samples corresponding to magnetite.

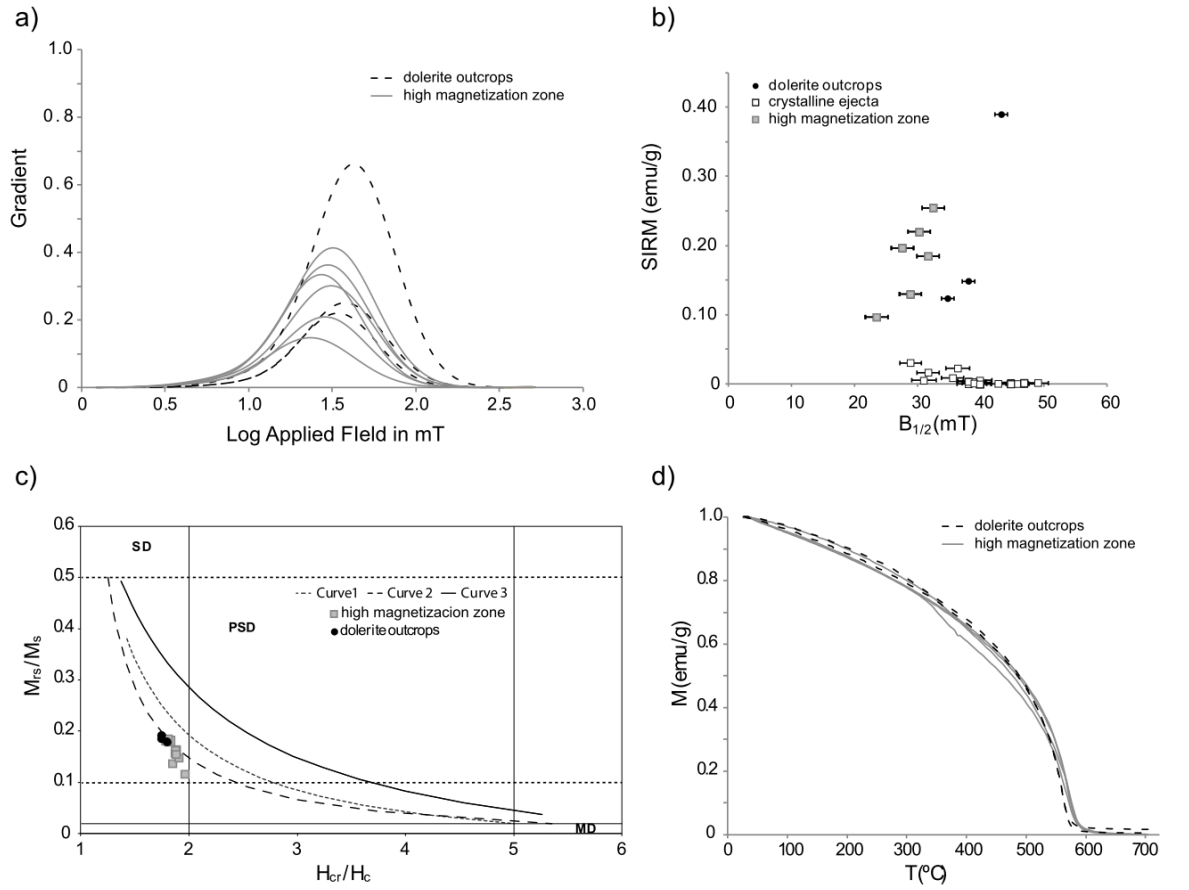

Figure 13. Comparison between the high magnetization zone from the Lockne-9 core (between 11.40 and 12.50m) and reference measurements from dolerite outcrops in the vicinity of Lockne crater. a) Coercivity spectra of IRM curves where dashed lines represent measurements from the dolerite outcrops and solid lines represent measurements from the anomalous zone in the core. b) Synthetic IRM versus $B_{1/2}$ of the main magnetic components, c) Day plot, and d) Heating curve of the magnetization as function of temperature between 0 and 700ºC. Dashed lines represent samples from Lockne dolerite outcrops and solid lines represent measurements from the anomalous zone in Lockne-9 core.

Table 2. Hysteresis parameters from the unaffected dolerite samples.

Sample	M_s (Am^2/kg)	M_r (Am^2/kg)	H_c (mT)	H_{cr} (mT)	K_{para} (m^3/kg)	K_{int} (m^3/kg)	M_r/M_s	H_{cr}/H_c
LOCDOL4	0.90	0.16	17.04	30.61	$9.05 \cdot 10^{-5}$	$5.70 \cdot 10^{-3}$	0.18	1.80
2012LD1	0.75	0.14	16.25	28.34	$9.27 \cdot 10^{-5}$	$5.08 \cdot 10^{-3}$	0.19	1.74
12LOC2	2.18	0.42	20.05	35.03	$1.78 \cdot 10^{-4}$	$1.21 \cdot 10^{-2}$	0.19	1.75

4. Discussion

The data presented here can be used in further analysis of the flap formation at Lockne. Of special significance are two pieces of information: i) typology of the ferromagnetic minerals and ii) their location along the core.

The magnetic mineralogy of the investigated core is clearly related to the presence of magnetite/titanomagnetite particles (Figures 4-8). In particular, the highest values of saturation magnetization obtained in the core are around 1.5 Am^2/kg and if we compare with the value for pure magnetite 92Am^2/kg (Dunlop and O□zdemir, 1997) we can estimate a magnetite content of 1.6%. Hysteresis derived parameters from the Lockne-9 core samples show a pronounced PSD behavior in the ejecta flap. As a consequence, the ferromagnetic phases found in this part of the core could slightly influence the values of the magnetic anomalies measured on the ground surface. On the other hand, the thermomagnetic curves reveal the presence of pyrite in some samples from the mixed zone (**Error! Reference source not found.**c) and in one sample from the ejecta flap at 17.08m depth (see supplementary material). Pyrite is a paramagnetic mineral that can have associated ferromagnetic phases of iron sulphates like pyrrhotite. The presence of pyrite has been observed in other rock magnetic studies at impact craters, e.g., Chesapeake Bay (Elbra et al., 2009), and the mineral is particularly interesting also due to its shock demagnetization behavior (Louzada et al., 2010).

The apparent absence of goethite suggests no hydrothermal alteration or weathering of previously existing ferromagnetic phases. Magnetite and titanomagnetite particles also show no indications of alteration that would be observed in the presence of maghemite in the thermomagnetic curves, which reinforces the scenario of a fast process.

The fractured and brecciated basement stands out from the rest of the core with regards to the location of ferromagnetic minerals. Low or even negative susceptibility values were measured for this lithology as well as the mixed zone. This indicates the presence of paramagnetic minerals (**Error! Reference source not found.**d). These results are supported by the thermomagnetic curves for samples from this part of the core (**Error! Reference source not found.**d). These observations imply that no significant amount of elements needed for ferromagnetic mineralization was transported through the fractures produced during the cratering process.

In addition to the differences observed between the brecciated basement and the overlying mixed zone and ejecta is a conspicuous anomaly occurring between 11.40 and 12.50m in the paramagnetic and bulk susceptibility (**Error! Reference source not found.**a and c) and in the magnetization parameters (**Error! Reference source not found.**a and b) within the crystalline ejecta. This coincides with the transition from the coarser grained mafic rock to the finer grain greenish mafic rock inside the ejecta flap.

We propose two different hypotheses for how this maximum can be interpreted i) values represent primary variations in the target before emplacement and ii) values represent alteration of the rock after the redeposition as impact ejecta. This second scenario would

imply processes such as hydrothermal diagenesis, low temperature transformation (maghemitization), and/or weathering.

We have developed the rationale of the current results in the frame of the two hypotheses based on three different rock magnetic experiments:

1. Coercivity spectra show only one significant component with a dispersion parameter (DP) of around 0,25 in the high magnetization zone (between 11.40 and 12.50m) suggesting no significant alteration in the magnetic fraction that would widen up the coercivity distributions (Egli, 2004b).
2. Thermomagnetic curves show no diagnosis of maghemite, a mineral that is highly unstable upon heating with a rupture zone is produced around 300ºC and a Curie temperature is about 600ºC (Dunlop and O□zdemir, 1997). Results from Figure 8 do not suggest the presence of maghemite in the analyzed lithologies.
3. Consistency with the rock magnetic properties measured for sporadic dolerite sills within the crystalline basement at the crater. Comparison of the coercivity spectra reveals a similar behavior of the magnetic population between the high magnetization zone from the Lockne-9 mafic rock (11.40-12.50m) and dolerite samples in the vicinity of the impact crater (**Error! Reference source not found.** a and b). The only observed discrepancy is a slight weakening in the coercivity of magnetic minerals of the core samples with respect to the rocks not affected by the impact (**Error! Reference source not found.**a and b). Thermomagnetic curves show that the composition remains however the same (Figure 13d).

Altogether, the data is in favor of the first hypothesis that the observed variations in grain size and magnetic properties of the mafic rock are primary. This implies that, although severely brecciated, the mafic part of the ejecta at the location of Lockne-9 is a fragment of rock that has been brecciated by the impact, but emplaced by the ejecta flow as a coherent body. The observed variations in grain size would be from the cooling and crystallization of the original intrusion (coarser towards the more slowly cooled center of the intrusion), and the magnetic variation a reflection of this cooling or an effect of changes occurring with time. Based on the standard relation between ballistic ejecta at the crater rim and the distance from where it would have travelled within the crater (e.g. Melosh, 1989) we can estimate that the mafic ejecta would originate from somewhere near the pre-impact shear zone that has been suggested to pass the center of the crater (Högström et al., 2010).

This model has implications for our understanding how material, although suffering strong brecciation, may be emplaced and ejected without major blending during the cratering.

5. Conclusions

The visual core log shows the crystalline flap to be mainly a brecciated mafic rock, likely an altered and subsequently ejected dolerite, with some blending with sedimentary target rock (Cambrian alum shale) just at the contact between the ejecta and the more intact granitic basement.

Different lithologies can be distinguished by measuring their paramagnetic susceptibility.

The ferromagnetic phases found in the Lockne-9 core are mainly magnetite/titanomagnetite, recognized by their thermomagnetic and IRM acquisition curves. Together with other encountered ferromagnetic phases associated with pyrite should be studied in more detail as they can potentially carry a stable remanent magnetization. Such studies will provide better constraints for future magnetic surveys of the Lockne crater.

The thermomagnetic curves combined with the coercivity spectra confirm that a distinct magnetic anomaly observed in the susceptibility and magnetization measurements is a primary feature already existing in the mafic rock before ejecta emplacement. A comparison with magnetic properties of dolerites unaffected by the impact indicates that this mafic rock most likely belongs to suite of known dolerites in the Lockne area. The observed rock magnetic and geochemical alterations support an ejection of this rock from somewhere within the distinct N-S trending shear zone that got hit by the impact. During the cratering process, this body was transported with the material of the growing cavity until it ended up at its current location within the crystalline ejecta flap.

This emphasizes how rock magnetic properties may be helpful to determine if an ejecta body, even though severely brecciated, has moved as finite particles or *en masse*, information that is of paramount importance for the understanding of the cratering process.

Rock magnetic data for comparison between the high magnetization zone from Lockne-9 core (between 11.40 and 12.50m) and reference dolerite outcrops in the vicinity of Lockne crater.

Acknowledgments

The manuscript has benefit from many colleagues, we would like to thank laboratory assistance by S. Guerrero-Suarez and V. Villasante from the UCM and M. P. Martín Redondo and M. T. Rodríguez-Sampedro from the CAB. IMA and JO are partially supported by the grants AYA2008-03467/ESP and AYA2011-24780-ESP. FMH has been partially supported by a Ramón y Cajal contract, all from the Spanish Ministry of Economy Competitiveness.

REFERENCES

Bertin, E.P., 1975. Principles and practice of X-ray spectrometric analy sis. Plenum Press,New York.

Butler, R.F., 1992. Paleomagnetism: magnetic domains to geologic terranes. Blackwell Scientific Publications.

Day, R., Fuller, M., Schmidt, V., 1977. Hysteresis properties of titanomagnetites: grain-size and compositional dependence. Phys. Earth Planet. Inter. 13, 260–267.

Dekkers, M., 1988. Magnetic behavior of natural goethite during thermal demagnetization. Geophys. Res. Lett. 15, 538–541.

Dunlop, D., O□zdemir, O., 1997. Rock magnetism: fundamentals and frontiers, Cambridge Studies in Magnetism. Cambridge University Press, Cambridge.

Dunlop, D.J., 2002a. Theory and application of the Day plot (Mrs/Ms versus Hcr/Hc) 1. Theoretical curves and tests using titanomagnetite data. J. Geophys. Res. Solid Earth 1978–2012 107, EPM–4.

Dunlop, D.J., 2002b. Theory and application of the Day plot (Mrs/Ms versus Hcr/Hc) 2. Application to data for rocks, sediments, and soils. J. Geophys. Res. Solid Earth 1978–2012 107, EPM–5.

Dunlop, D.J., 2002c. Theory and application of the Day plot (Mrs/Ms versus Hcr/Hc) 1. Theoretical curves and tests using titanomagnetite data. J. Geophys. Res. Solid Earth 1978–2012 107, EPM–4.

Egli, R., 2004a. Characterization of individual rock magnetic components by analysis of remanence curves, 1. Unmixing natural sediments. Stud. Geophys. Geod. 48, 391–446.

Egli, R., 2004b. Characterization of individual rock magnetic components by analysis of remanence curves.: 2. Fundamental properties of coercivity distributions. Phys. Chem. Earth Parts ABC 29, 851–867.

Elbra, T., Kontny, A., Pesonen, L., 2009. Rock-magnetic properties of the ICDP-USGS Eyreville core, Chesapeake Bay impact structure, Virginia, USA. ICDP-USGS Deep Drill. Proj. Chesap. Bay Impact Struct. Results Eyreville Core Holes Geol. Soc. Am. Spec. Pap. 458.

Frisk, Å.M., Ormö, J., 2007. Facies distribution of post-impact sediments in the Ordovician Lockne and Tvären impact craters: Indications for unique impact-generated environments. Meteorit. Planet. Sci. 42, 1971–1984.

Heslop, D., Dekkers, M.J., Kruiver, P.P., Van Oorschot, I.H.M., 2002. Analysis of isothermal remanent magnetization acquisition curves using the expectation–maximization algorithm. Geophys. J. Int. 148, 58–64.

Heslop, D., McIntosh, G., Dekkers, M.J., 2004. Using time- and temperature-dependent Preisach models to investigate the limitations of modelling isothermal remanent magnetization acquisition curves with cumulative log Gaussian functions. Geophys. J. Int. 157, 55–63.

Högström, A.E., Sturkell, E., Ebbestad, J.O.R., Lindström, M., Ormö, J., 2010. Concentric impact structures in the Palaeozoic of Sweden–the Lockne and Siljan craters. GFF 132, 65–70.

Jasonov, P., Nourgaliev, D., Burov, B., Heller, F., 1998. A modernized coercivity spectrometer. Geol. Carpathica 49, 224–226.

Kruiver, P.P., Dekkers, M.J., Heslop, D., 2001. Quantification of magnetic coercivity components by the analysis of acquisition curves of isothermal remanent magnetisation. Earth Planet. Sci. Lett. 189, 269–276.

Lindgren, P., Parnell, J., Norman, C., Mark, D.F., Baron, M., Ormö, J., Sturkell, E., Conliffe, J., Fraser, W., 2007. Formation of uranium-thorium-rich bitumen nodules in the Lockne impact structure, Sweden: A mechanism for carbon concentration at impact sites. Meteorit. Planet. Sci. 42, 1961–1969.

Lindström, M., Ormö, J., Sturkell, E., Dalwigk, I., 2005. The Lockne Crater: Revision and Reassessment of Structure and Impact Stratigraphy, in: Koeberl, C., Henkel, H. (Eds.), Impact Tectonics, Impact Studies. Springer Berlin Heidelberg, pp. 357–388.

Lindström, M., Shuvalov, V., Ivanov, B., 2005. Lockne crater as a result of marine-target oblique impact. Planet. Space Sci. 53, 803–815.

Louzada, K.L., Stewart, S.T., Weiss, B.P., Gattacceca, J., Bezaeva, N.S., 2010. Shock and static pressure demagnetization of pyrrhotite and implications for the Martian crust. Earth Planet. Sci. Lett. 290, 90–101.

Lowrie, W., 1990. Identification of ferromagnetic minerals in a rock by coercivity and unblocking temperature properties. Geophys. Res. Lett. 17, 159–162.

Melosh, H.J., 1989. Impact cratering: a geologic process, Oxford monographs on geology and geophysics. Oxford University Press.

Moskowitz, B.M., 1981. Methods for estimating Curie temperatures of titanomaghemites from experimental< i> Js-T</i> data. Earth Planet. Sci. Lett. 53, 84–88.

O'Reilly, W., 1976. Magnetic minerals in the crust of the Earth. Rep. Prog. Phys. 39, 857.

Ormö, J., Hill, A.C., Self-Trail, J.M., 2010. A chemostratigraphic method to determine the end of impact-related sedimentation at marine-target impact craters (Chesapeake Bay, Lockne, Tväreń). Meteorit. Planet. Sci. 45, 1206–1224.

Ormö, J., Lindström, M., 2000. When a cosmic impact strikes the sea bed. Geol. Mag. 137, 67–80.

Ormö, J., Lindström, M., 2005. New Drill-Core Data from the Lockne Crater, Sweden: The Marine Excavation and Ejection Processes, and Post-Impact Environment, in: 36th Annual Lunar and Planetary Science Conference. p. 1124.

Özdemir, Ö., Dunlop, D.J., 2000. Intermediate magnetite formation during dehydration of goethite. Earth Planet. Sci. Lett. 177, 59–67.

Rochette, P., 1987. Magnetic susceptibility of the rock matrix related to magnetic fabric studies. J. Struct. Geol. 9, 1015–1020.

Shuvalov, V., Ormö, J., Lindström, M., 2005. Hydrocode Simulation of the Lockne Marine Target Impact Event, in: Koeberl, C., Henkel, H. (Eds.), Impact Tectonics, Impact Studies. Springer Berlin Heidelberg, pp. 405–422.

Sturkell, E., Lindström, M., 2004. The target peneplain of the Lockne impact. Meteorit. Planet. Sci. 39, 1721–1731.

Sturkell, E., Ormö, J., Lepinette, A., 2013. Early modification stage (preresurge) sediment mobilization in the Lockne concentric, marine-target crater, Sweden. Meteorit. Planet. Sci. 48, 321–338.

Sturkell, E.F., Ormö, J., 1997. Impact-related clastic injections in the marine Ordovician Lockne impact structure, Central Sweden. Sedimentology 44, 793–804.

Sturkell, E.F., Ormö, J., 1998. Magnetometry of the marine, Ordovician Lockne impact structure, Jämtland, Sweden. J. Appl. Geophys. 38, 195–207.

Sturkell, E.F.F., 1998. The marine Lockne impact structure, Jämtland, Sweden: a review. Geol. Rundsch. 87, 253–267.

Sturkell, E.F.F., Ekelund, A., Törnberg, R., 1998. Gravity modelling of Lockne, a marine impact structure in Jämtland, central Sweden. Tectonophysics 296, 421 – 435.

Törnberg, R., Sturkell, E.F.F., 2005. Density and magnetic susceptibility of rocks from the Lockne and Tvären marine impact structures. Meteorit. Planet. Sci. 40, 639–651.

Supplementary material

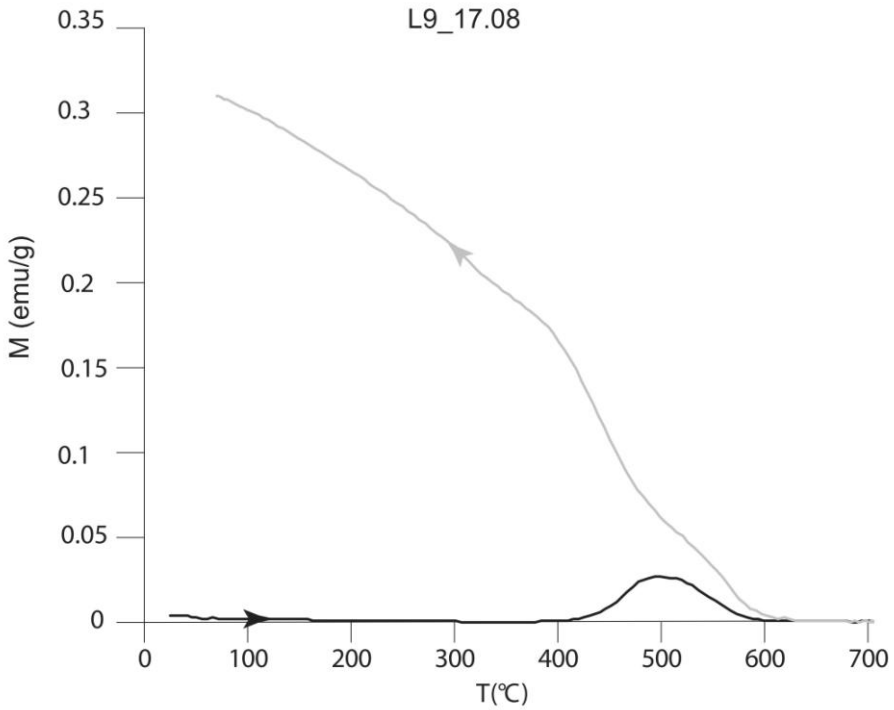

Figure 14. Thermomagnetic curve of a sample enriched in pyrite with evidences of pyrite transformation between 400 and 600ºC in the heating transect (dark curve).

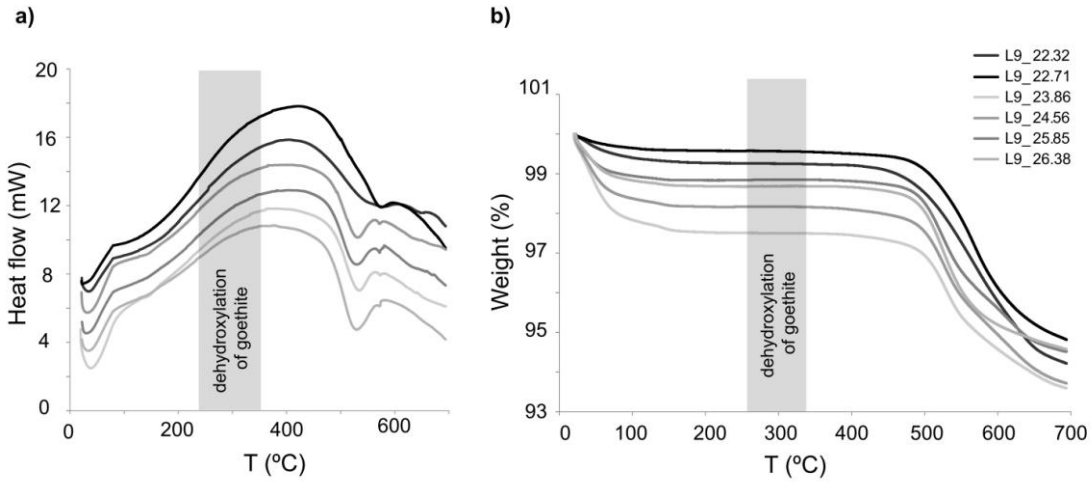

Figure 155. Representation of the dependence of the a) heat flow and b) weight loss with temperature for six representative samples of the Lockne-9 core. The shadowed area corresponds to the dehydroxilation temperature range of goethite.